# History matching and production optimization under uncertainties – Application of closed-loop reservoir management

Vinícius Luiz Santos Silva [a,*], Alexandre Anozé Emerick [a], Paulo Couto [b], José Luis Drummond Alves [b]

[a] *Petrobras, Brazil*
[b] *Universidade Federal do Rio de Janeiro, Brazil*

ABSTRACT

There is an intensive investigation reported in the literature regarding the development of robust methods to improve the economical performance during the production management of petroleum fields. One paradigm that emerged in the last decade and has been calling the attention of various research groups is known as closed-loop reservoir management. The closed-loop entails the application of history matching and production optimization in a near-continuous feedback process. This work presents a closed-loop workflow constructed with ensemble-based methods. The proposed workflow consists of three components: history matching, model selection and production optimization. For history matching, we use the method known as ensemble smoother with multiple data assimilation. For model selection, we propose a procedure grounded on the calculation of distances defined in a metric space and a minimization procedure to determine the optimal set of representative models. For production optimization, we use the ensemble-based optimization method. We investigate the performance of each method separately before testing the complete closed-loop in a benchmark problem based on Namorado field in Campos Basis, Brazil. The results showed the effectiveness of the proposed methods to form a robust closed-loop workflow.

## 1. Introduction

Recent advances in geological modeling and reservoir simulation have changed several aspects of the history-matching practice leading to a dramatic increase in research and development in this area. The purpose of history matching evolved from finding a single "best" set of model parameters to finding multiple history-matched models that can be used to quantify uncertainty in production forecast (Oliver and Chen, 2011). Among the recent advances in history matching great focus has been given to the ensemble Kalman filter (EnKF) (Evensen, 1994) and its variants. See, for example, Aanonsen et al. (2009) and Oliver and Chen (2011) for a review of applications of EnKF in the context of reservoir history matching. EnKF is a Monte Carlo version of the Kalman filter (Kalman, 1960) which uses a set of model realizations (ensemble) to assimilate data sequentially in time. Another method based on the Kalman filter is the ensemble smother (ES), which was introduced by van Leeuwen and Evensen (1996). The first application of ES for history matching was presented by Skjervheim et al. (2011). ES is an alternative for history matching that differs from EnKF by not assimilating data sequentially in time. For ES, we have a single update with all available

data. This fact makes ES significantly faster and easies to implement in practical applications than EnKF. However, recent results reported in the literature indicate that ES fails to obtain acceptable data matches (Chen and Oliver, 2012; Emerick and Reynolds, 2013a,b). Inspired by the idea of using "duplicated measurements" presented by Rommelse (2009), Emerick and Reynolds (2013b) proposed the ensemble smoother with multiple data assimilation (ES-MDA) aiming to improve the history-matching results obtained by the ES. The basic idea behind ES-MDA is to assimilate the same set of data multiple times, mimicking an iterative process. Emerick and Reynolds (2013a) showed that for a simplistic, but highly nonlinear history-matching problem, ES-MDA achieved the best results in terms of both data matches and quantification of uncertainty when compared to several other ensemble-based methods.

A clear advantage of the ensemble-based methods is the fact that they generate a set of conditional realizations which can be used for uncertainty quantification. However, in practical terms, it may not be feasible to analyze, interpret and optimize a large number of realizations. Therefore, for decision making, it is necessary to work with a small representative subset of these models. Ideally, this subset of models should be selected such that the same decision considering the whole

---

ensemble is maintained when analyzed only the subset of models. The problem of making this selection is usually referred to as "scenario reduction" or "selection of representative models" in the literature. A traditional strategy used in the industry is to rank models based in a single decision variable. For example, select the models closest to pre-defined percentiles (Ballin et al., 1992); say, P10, P50 and P90 of the net present value (NPV). The major shortcoming of this strategy is the limited predictive ability of models selected based on a single criterion when the operational conditions change. In order to improve the representativeness of the selected models, Schiozer et al. (2004) proposed a qualitative procedure to use multiple decision variables in the selection process. Scheidt and Caers (2009a,b) proposed a quantitative approach based on calculating distances between all pairs of models which are mapped to a low-dimensional space where a cluster analysis is applied. Shirangi and Durlofsky (2016) also investigated the model selection problem. They proposed a procedure which combines permeability-based and flow-based quantities and clustering algorithms. Meira et al. (2016) proposed an approach based on the minimization of a multi-objective function considering cross-plots of the main output variables, risk curves and attribute-levels of the problem. Another approach based on optimization was proposed by Heitsch and Römisch (2003) where the selection problem is formalized in terms of minimizing the weight of the discarded models. This method was extended and applied to geostatistics by Armstrong et al. (2013) and to energy planning by Oliveira et al. (2010).

There is an increasing number of publications devoted to the development and application of optimization methods to improve the economical performance of oil and gas fields. Several numerical methods are available to solve this maximization problem. One efficient alternative is the application of methods which use the gradient of the objective function to guide the iterative process (Nocedal and Wright, 2006). However, gradient-based methods are computationally efficient for production optimization only when the adjoint method is implemented in the reservoir simulator; see, e.g., (Sarma et al., 2008a; Jansen, 2011; Chen et al., 2012). Unfortunately, this implementation is costly, it requires a great knowledge of the numerical simulator code and it is usually not available in commercial simulators. For this reason, there is an intensive research activity to develop efficient approximate-gradient methods for production optimization. It appears that the first work to use approximate gradients in the context of production optimization was presented by Lorentzen et al. (2006) who proposed an optimization method based on EnKF. This idea was also supported by the work from Reynolds et al. (2006), who showed that the EnKF update is similar to one Gauss-Newton iteration. Later, Chen et al. (2009) made improvements in this method and coined the name EnOpt (ensemble-based optimization). Do and Reynolds (2013) showed that EnOpt can be derived as a special case of a smoothed version of the simultaneous perturbation stochastic approximation (SPSA) (Spall, 1992, 1998). In fact, the same authors concluded that both algorithms resulted in similar estimates of NPV for a small production optimization problem.

Production optimization methods rely on predictions from reservoir simulation models to define operational strategies that maximizes production and/or reduce costs. However, reservoir models are built based on limited information, which makes their predictions uncertain. Therefore, it is necessary to formally consider the uncertainty during optimizations to manage risk. On the other hand, continuous measurements of pressure and flow rate at wells obtained during the field operation can help to mitigate uncertainty through history matching. The application of history matching and production optimization under uncertainties in a near-continuous process throughout the productive life of the field is known in the petroleum literature as closed-loop reservoir management (CLRM) (Brouwer et al., 2004; Sarma et al., 2005; Wang et al., 2009; Jansen et al., 2009).

In this work, we propose a closed-loop workflow and evaluate its performance in a benchmark problem based on Namorado field in Campos Basin, Brazil. The workflow is composed by three elements:

history matching, model selection and production optimization. For history matching, we use ES-MDA. For model selection, we propose a procedure based on the work of Heitsch and Römisch (2003). For optimization, we use EnOpt to maximize the expected field NPV. The remaining of the paper is organized as follows: the next section introduces the benchmark problem (UNISIM-I case). Then, we present the results of ES-MDA for history matching. After that, we present the procedure for model selection followed by the results of EnOpt for production optimization. Finally, we present the proposed CLRM workflow and show the results for the UNISIM-I case. The last section of the paper presents the conclusions.

## 2. UNISIM-I case

UNISIM-I is a benchmark problem introduced by (Avansi and Schiozer, 2015) to evaluate different methodologies related to field development and reservoir management. In the benchmark there is a reference model, called UNISIM-I-R, which can be regarded as the "real reservoir," so that the performance of different methodologies can be compared. The UNISIM-I-R is based on actual data from Namorado Field. It was built with a high level of geological details. The model is discretized into a corner-point grid with $326 \times 234 \times 157$ gridblocks with dimensions $25 \times 25 \times 1$ meters. The total number of active gridblocks is on the order of 3.5 millions. A detailed description regarding the construction of the UNISIM-I-R model can be found in (Avansi and Schiozer, 2015).

The benchmark problem also includes a coarse-scale model called UNISIM-I-D. This model was constructed with only a small subset of the information used to build UNISIM-I-R (Avansi and Schiozer, 2015). The UNISIM-I-D was created to represent a model of a field in an early stage of development, when only four vertical production wells had been drilled. The model was discretized into a corner-point grid with $81 \times 58 \times 20$ gridblocks, with dimensions $100 \times 100 \times 8$ meters and 37,000 active gridblocks. A total of 500 realizations of the UNISIM-I-D model were built based on the data from these four wells and a 3D seismic (Gaspar et al., 2015). Fig. 1 shows the porosity distribution of the first layer of the model UNISIM-I-R and the first layer of the first realization of UNISIM-I-D. This figure illustrates the significant contrast of grid resolution between the two models. Note, for example, that the UNISIM-I-R has a much higher contrast of porosity than UNSIM-I-D.

Originally, the UNISIM-I benchmark was designed as a field development problem, i.e., the objective is to define the optimal well placement strategy to exploit the field. An initial exploitation strategy with four wells producing for a period of four years was available. The objective of the benchmark is to define the production strategy from year four to year 30. A detailed description of the benchmark can be found in (Gaspar et al., 2015). Here, because our objective is to test a CLRM workflow, we consider a slightly modified version of the benchmark. We use a fixed well placement based on 25 wells (4 original vertical producers, 10 horizontal producers and 11 injectors). This well configuration is the same proposed by (Avansi and Schiozer, 2015). For each well, we consider two independent inflow control valves (ICV). Fig. 2 shows the position of the wells. Note that this figure shows the position of the wells projected in the first layer of the model. The actual wells are perforated in different layers of the model, typically water injectors are perforated in bottom while oil producing wells are perforated in the top of the reservoir.

Unlike the original benchmark problem, here we evaluate the performance of the proposed CLRM workflow to maximize the field NPV over a period of 30 years divided into six closed-loop cycles. Each cycle comprises a production period, followed by a history matching and selection of representative models for optimization. We write the NPV as $\mathscr{J}(\mathbf{m}, \mathbf{u})$, which is a function of the vector of uncertain model parameters, $\mathbf{m}$, and the vector production controls (decision variables), $\mathbf{u}$. The NPV is computed as
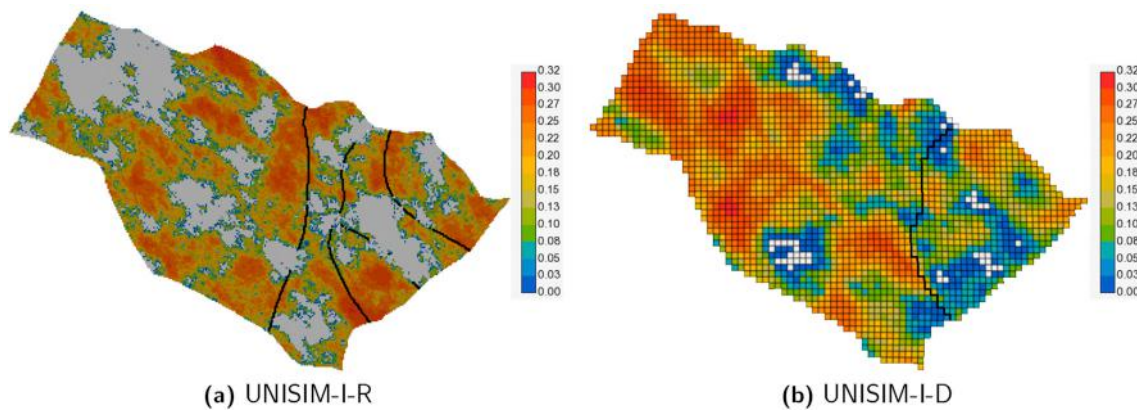
**Fig. 1.** Porosity distribution of the first layer of UNISIM-I-R and one realization of UNISIM-I-D. The blank areas in the figures indicate regions with inactive gridblocks (i.e., no reservoir).
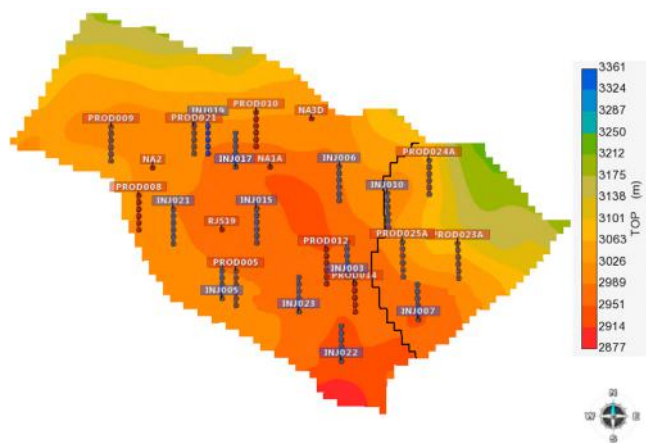


**Fig. 2.** Depth of the top of the reservoir showing the position of the wells.

$$\mathscr{J}(\mathbf{m}, \mathbf{u}) = \sum_{n=1}^{N_t} \frac{Q_o^n(\mathbf{m}, \mathbf{u})\Delta t_n}{(1+\gamma)^n}, \tag{1}$$

where $Q_o^n(\mathbf{m}, \mathbf{u})$ is oil production rate over a period $\Delta t_n$, $N_t$ in the number of time steps and $\gamma = 0.1$ is the discount rate. Note that our NPV corresponds to a simple discounted cumulative oil production. This is clearly a simplification which is very usual in real-life reservoir management problems where the focus is primarily in maximize oil production. Note that the total water production and injection is constrained internally using controls from the reservoir simulator. Therefore, maximization of oil production will not generate a solution that requires water production or injection beyond the specified production unity capacity.

## 3. History matching

In this section, we investigate the performance of ES-MDA for history matching the UNISIM-I case. The observed data correspond to monthly measurements of oil rate, water cut, gas-oil ratio and bottom-hole pressure for the oil producing wells, and water rate and bottom-hole pressure for the injection wells. In order to mimic real measurements, we added a random Gaussian noise to the data predicted by UNISIM-I-R to obtain the data used for history matching. The standard deviation used to compute the noise of the observed data corresponds to 5% for oil rate, 5% for water rate, 10% for gas rate and 3 kgf/cm$^2$ for bottom-hole pressure.

The parameters used for the history matching are the same described in the original benchmark problem. We can divide these parameters in two types: grid and scalar parameters. The grid parameters include horizontal permeabilities ($\mathbf{k}_I$ e $\mathbf{k}_J$), vertical permeability ($\mathbf{k}_K$), porosity

($\phi$) and net-to-gross ratio (**ntg**). The prior uncertainty in these parameters is represented by 500 initial geological realizations. The scalar parameters include a vertical permeability multiplier (MULTK), a critical water saturation (SWCR), a water relative permeability endpoint (KRWMAX), rock compressibility (CPOR) and the depth of water-oil contact of the East Block (WOC2), which is the block in the right side of the fault shown in Fig. 2. The prior uncertainty in the scalar parameters is represented by triangular distributions with minimum, maximum and mode listed in Table 1. The rock compressibility is given in $(\text{kgf/cm}^2)^{-1}$ and depth of water-oil contact in meters. It is worth mentioning that in the construction of the UNISIM-I-D model there was no upscaling of relative-permeability curves. Instead, the authors of the benchmark followed a more direct approach which consisted of introducing uncertainty in the relative permeability directly in the course scale model. One consequence of this approach is that the relative permeability curves that best match data in the coarse scale may not be the same as the one in the original fine grid.

ES-MDA requires to define the number of data assimilations in advance. The results presented in (Emerick and Reynolds, 2013b,c; Emerick, 2016; Maucec et al., 2016) indicate that few data assimilations suffice for practical history-matching problems. Here, we use four data assimilations which is our typical choice. In order to improve the quality of the results, we apply localization of the Kalman gain (Emerick and Reynolds, 2011b, a) to update the grid parameters. The correlation length for localization was defined as a constant radius of 2000 m for all data points. This choice is based on our previous experience with other history matching problems. We did not investigate the effect of this choice in the history-matching results. The correlation function used is the well-known Gaspari-Cohn correlation (Gaspari and Cohn, 1999). The ES-MDA updating equation at the $k$th data assimilation step can be written in a compact form as

**Table 1**
Prior distribution for the scalar parameters.

| Scalar parameters | Minimum | Mode | Maximum |
|---|---|---|---|
| MULTK | 0.0 | 1.5 | 3.0 |
| SWCR | 0.30 | 0.35 | 0.40 |
| KRWMAX | 0.15 | 0.35 | 0.55 |
| CPOR | $1.0 \times 10^{-5}$ | $5.3 \times 10^{-5}$ | $9.6 \times 10^{-5}$ |
| WOC2 | 3024 | 3174 | 3324 |

**Table 2**
Mean squared error between simulated and observed data.

| | Minimum | Average | Maximum |
|---|---|---|---|
| Prior ensemble | 12.2 | 145.5 | 5634.8 |
| Posterior ensemble | 5.7 | 6.2 | 9.2 |

$$\mathbf{m}_j^{k+1} = \mathbf{m}_j^k + \mathbf{R} \circ \left[ \mathbf{C}_{\mathbf{md}}^k \left( \mathbf{C}_{\mathbf{dd}}^k + \alpha_k \mathbf{C}_{\mathbf{d}} \right)^{-1} \right] \left( \mathbf{d}_{\mathrm{obs}} - \mathbf{g} \left( \mathbf{m}_j^k \right) + \varepsilon_j^k \right), \tag{2}$$

for $j = 1, \ldots, N_e$, with $N_e$ denoting the size of the ensemble. Here, $N_e = 500$. In the above equation, $\mathbf{m}$ is the vector of model parameters and $\mathbf{R}$ is the correlation matrix used for localization of the Kalman gain, which is accomplished with the Schur product denoted by "$\circ$". $\mathbf{C}_{\mathbf{md}}$ is the covariance between model and predicted data and $\mathbf{C}_{\mathbf{dd}}$ is the covariance matrix of predicted data. Both matrices are estimated based on the current ensemble. $\mathbf{C}_{\mathbf{d}}$ is the covariance matrix of the observed data measurement errors, which in the ES-MDA method is "inflated" by a multiplication with the coefficient $\alpha > 0$. The selection of $\alpha$ is somewhat arbitrary as long as the following condition holds

$$\sum_{k=1}^{N_a} \frac{1}{\alpha_k} = 1, \tag{3}$$

where $N_a$ is the number of data assimilations. Here, we use $\alpha_k = N_a = 4$ for $k = 1, \ldots, N_a$. In Eq. (2), $\mathbf{d}_{\mathrm{obs}}$ is the vector containing the observed data and $\mathbf{g}(\mathbf{m})$ is the corresponding vector of predicted data. $\varepsilon$ is a random vector obtained by sampling a normal distribution with zero mean and covariance given by $\alpha \mathbf{C}_{\mathbf{d}}$, i.e., $\varepsilon \sim \mathcal{N}(0, \alpha \mathbf{C}_{\mathbf{d}})$. Here, we constructed $\mathbf{C}_{\mathbf{d}}$ assuming that all measurement errors are uncorrelated in time and space, in which case we have a diagonal matrix with elements corresponding to the variance of the measurement errors. Moreover we assumed that there are no bias in the measurements. This last assumption is very common even in real-life applications despite the fact that real measurements are likely to contain some bias.

### 3.1. Data assimilation results

In order to investigate the performance of ES-MDA, we first consider the history-matching results for a production period of 9 years. Later, we compare the results for different data assimilation periods in terms of the posterior distribution of predicted field NPV.

Table 2 shows the mean squared error (MSE) between the simulated and measured data calculated for the 500 initial models (prior ensemble) and the 500 final models (posterior ensemble). The MSE of the $j$th model is computed as

$$\mathrm{MSE}_j = \frac{1}{N_d} \sum_{i=1}^{N_d} \left( \frac{d_{\mathrm{obs},i} - g_i(\mathbf{m}_j)}{\sigma_i} \right)^2, \tag{4}$$

where $N_d$ is the number of data points, $d_{\mathrm{obs},i}$ is the $i$th observed data point and $g_i(\mathbf{m}_j)$ is the corresponding predicted data. $\sigma_i$ is the standard deviation of the measurement error of the $i$th observed data point.

The results in Table 2 show that the posterior ensemble generated by ES-MDA achieved far superior data matches than the prior ensemble. For example, the average MSE was reduced by 24 times after data assimilation. Fig. 3 shows the simulated data before and after history matching compared with the observed data for one well of the field (PROD012). The history-matching results obtained for well PROD012 are representative of what is observed for most of the wells in the field. The results presented in Table 2 and Fig. 3 indicate that the data assimilation was very successful, at least in terms of reproducing the observed production data. These results demonstrate the robustness of the method ES-MDA, since satisfactory data matches were obtained without the need to define local or regional property multipliers which is still a quite common history-matching practice in the industry.

Fig. 4 shows the average among all layers of the model for the natural logarithm of horizontal permeability before and after data assimilation for the first three realizations of UNISIM-I-D. For comparisons, we also show the average log-permeability of UNISIM-I-R in this figure. We observe that the posterior realizations present some characteristics of the UNISIM-I-R model which are not present in the prior ones. On the other

hand, none of these realizations are able to reproduce the low permeability observed in the Northwest part of UNISIM-I-R. This is explained by the absence of wells in this region. In other words, there are no observed data to collect information about this area. At the same time, we can see that each final realization still retains some characteristics of the corresponding priors. In fact, this is a desirable feature of the method as one possible interpretation is that the method seeks for the minimum changes in the initial model parameters necessary to adjust the observed data (Oliver and Chen, 2011). Finally, it is important to note that the UNISIM-I case does not seem to be a particularly challenging problem in terms of geological complexity for history matching. The realizations of petrophysical properties present a near Gaussian behavior, which may explain the remarkable performance of the ES-MDA method in this problem.

### 3.2. Comparison between different historical periods

In this section, we compare the performance of the posterior ensemble obtained by ES-MDA in terms of the predicted NPV after 30 years of production considering six periods of historical data, denoted by $t1, \ldots, t6$. Fig. 5 shows the empirical cumulative distributions of NPV obtained with the ensembles before and after history matching. For comparisons, we also present the reference NPV obtained with UNISIM-I-R. The results in this figure indicate a significant reduction in the production forecast uncertainty after data assimilation. This is particularly evident for the cases with longer periods of history. Moreover, according to results of Fig. 5(a) and (b), the posterior ensembles obtained for the historical periods $t1$ and $t2$ predicted systematically higher NPV values than the prior ensemble. Furthermore, most of the posterior models also predicted higher NPV values than the UNISIM-I-R case. This situation is reverted for longer historical periods ($t3$ to $t6$).

We believe this happens because the initial permeability realizations of UNISIM-I-D are significantly smoother than the UNISIM-I-R model. In practice, we observe that smooth permeability fields tend to predict homogenous waterflooding resulting in late water breakthrough and, consequently, overestimating oil production. Moreover, until $t2$ there were not significant history of water production in the UNISIM-I-R. Consequently, the observed data were not enough to introduce significant heterogeneity in the permeability realizations of UNISIM-I-D. On the other hand, at $t3$ water breakthrough was observed in several wells bringing relevant information about the spatial distribution of transmissibility in the reservoir. As a result, the history matching was able to generate models with better predictions.

## 4. Model selection

In this section, we present the selection of representative models applied to UNISIM-I-D. We propose a procedure based on the works from Heitsch and Römisch (2003) and Armstrong et al. (2013). The method consists of constructing a metric space by defining "distances" between models. Then, the optimal selection is obtained by solving the following optimization problem

$$L = \arg \min_L \mathscr{C}(L),$$

$$\mathscr{C}(L) = \sum_{i \in \overline{L}} p_i \min_{j \in L} d(j, i), \tag{5}$$

where $L$ is a subset with the selected models, $\overline{L}$ is a subset with the non-selected models, $p_i$ is the probability of the model $i$ and $d(j, i)$ represent the distance between the $j$th and the $i$th models. $\mathscr{C}(L)$ can be regarded as the sum of the distances between the non-selected models and the closest selected one. For the probability of each model, we consider $p_i = 1/N_e$, $i = 1, \ldots, N_e$. In this work, we use a genetic algorithm (GA) to solve this optimization problem as proposed by Armstrong et al. (2014). Because
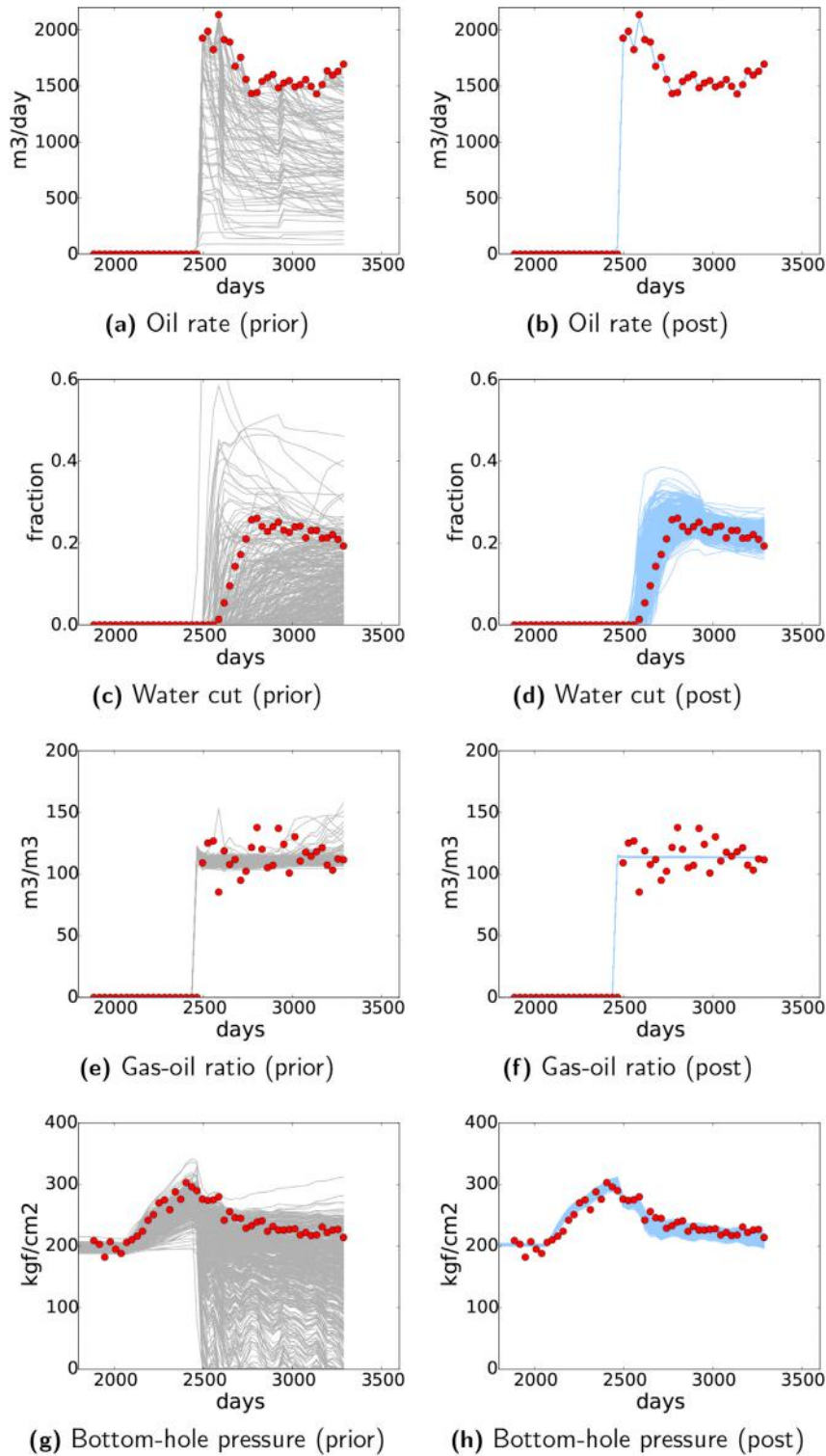
**Fig. 3.** Production data for well PROD012. Red circles are the observed data, gray and blue lines are the predicted data from the prior and posterior ensembles, respectively. (For interpretation of the references to colour in this figure legend, the reader is referred to the web version of this article.)

the objective function evaluation is almost inexpensive, we can afford to use GA with a large population size. Here, we use a population of 1000 individuals over a period of 100 generations.

The probability associated to each selected model, $q_j$, is calculated by adding the probabilities $p_i$ of the non-selected models closer to it plus the probability $p_j$ of that model, i.e.,

$$q_j = p_j + \sum_{i \in \overline{L}_j} p_i, \quad \text{where } \overline{L}_j = \left\{ i \in \overline{L} : j \in \arg\min_{j \in L} d(j, i) \right\}. \quad (6)$$

Typically, model selection is based only on output variables of a simulation, e.g., cumulative oil production or NPV. Here, in order to have a robust selection, we propose to select models based on the history-
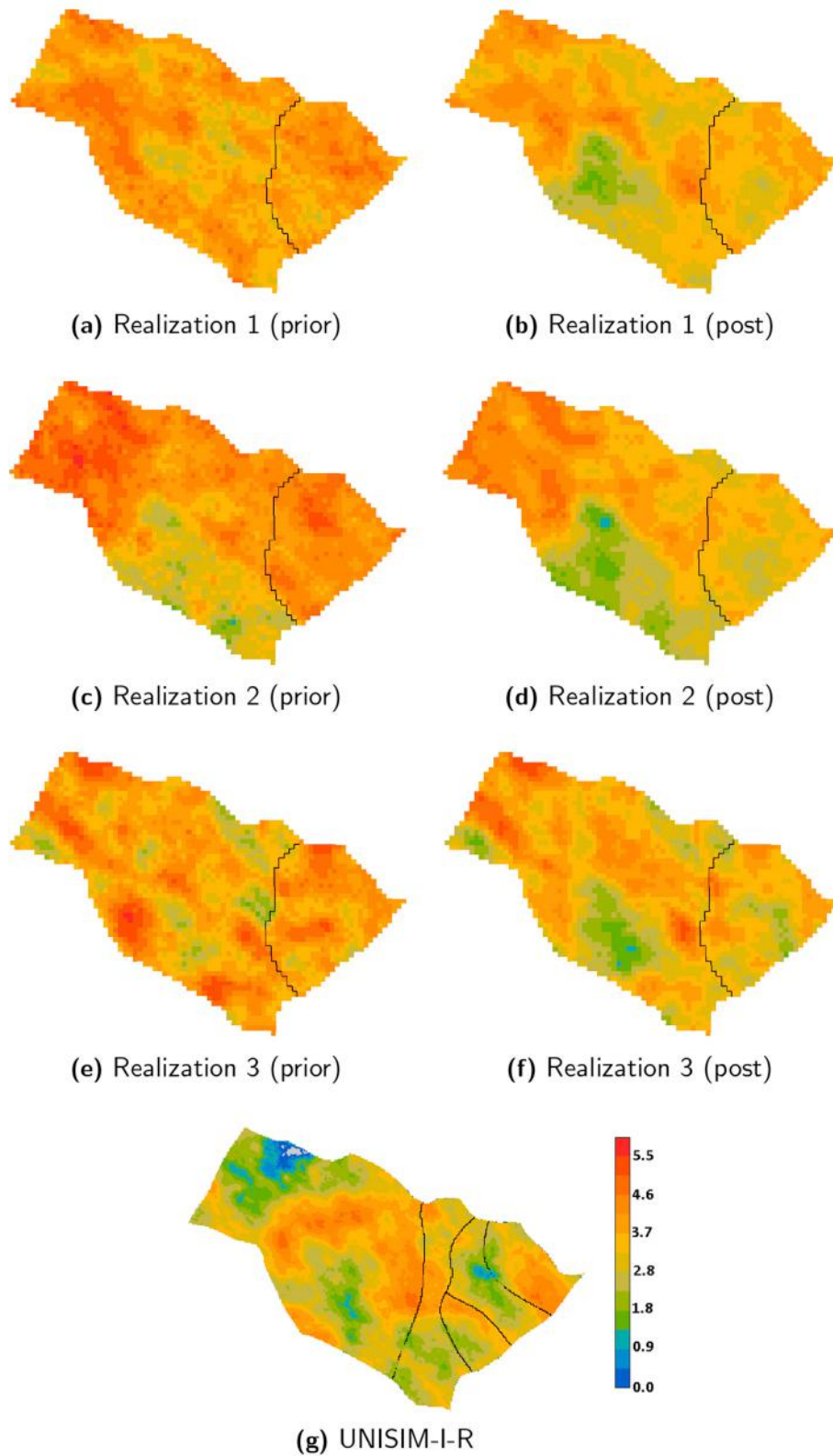
**(a)** Realization 1 (prior)

**(b)** Realization 1 (post)

**(c)** Realization 2 (prior)

**(d)** Realization 2 (post)

**(e)** Realization 3 (prior)

**(f)** Realization 3 (post)

**(g)** UNISIM-I-R

**Fig. 4.** Average log-permeability (in ln-mD) before and after data assimilation.

matching parameters (grid and scalar parameters) in addition to a set of production and volume variables. We represent the grid parameters in terms of their mean and standard deviation. Recall that the grid parameters include horizontal and vertical permeabilities, porosity and net-to-gross ratio. The scalar parameters are also the same used in the history matching (vertical permeability multiplier, critical water saturation, water relative permeability endpoint, rock compressibility and depth of water-oil contact of the East block). The volume variable is the original oil in place (OOIP), and the production variables include, cumulative oil production ($Np$), cumulative water production ($Wp$), oil recovery factor ($RF$) and NPV. Here, we refer to all model parameters and output variables simple as "selection variables."

The distance between two models is computed as

$$d(j,i) = \sqrt{\sum_{k=1}^{N_s} \left[ \omega_k \left( z_{j,k} - z_{i,k} \right) \right]^2}, \tag{7}$$

where $N_s$ is the number of selection variables; here, $N_s = 20$. $\omega$ is the weight attributed to each selection variable and $z$ is a standardized value for the selection variable computed by subtracting the mean and dividing by the standard deviation. For the UNISIM-I case, we have 15 selection variables corresponding to history-matching parameters, one selection variable corresponding to a volume parameter and four selection

variables corresponding to output from the flow simulator. Therefore, we selected the weights such that the sum of the weights for the history-matching parameters and the volume parameter is the same as the sum for the output variables. Moreover, among the output variables, we attributed a higher weight to the NPV since it is the objective function of the production optimization. Table 3 lists all selection variables with their respective (unnormalized) weights.

During the closed-loop workflow it is necessary to apply the model selection before each optimization cycle. Here, we show the results of the model selection after the first cycle, $t1$. This cycle corresponds to a five-years production period. We selected five representative models among the 500 posterior realizations. Table 4 shows the selected models with
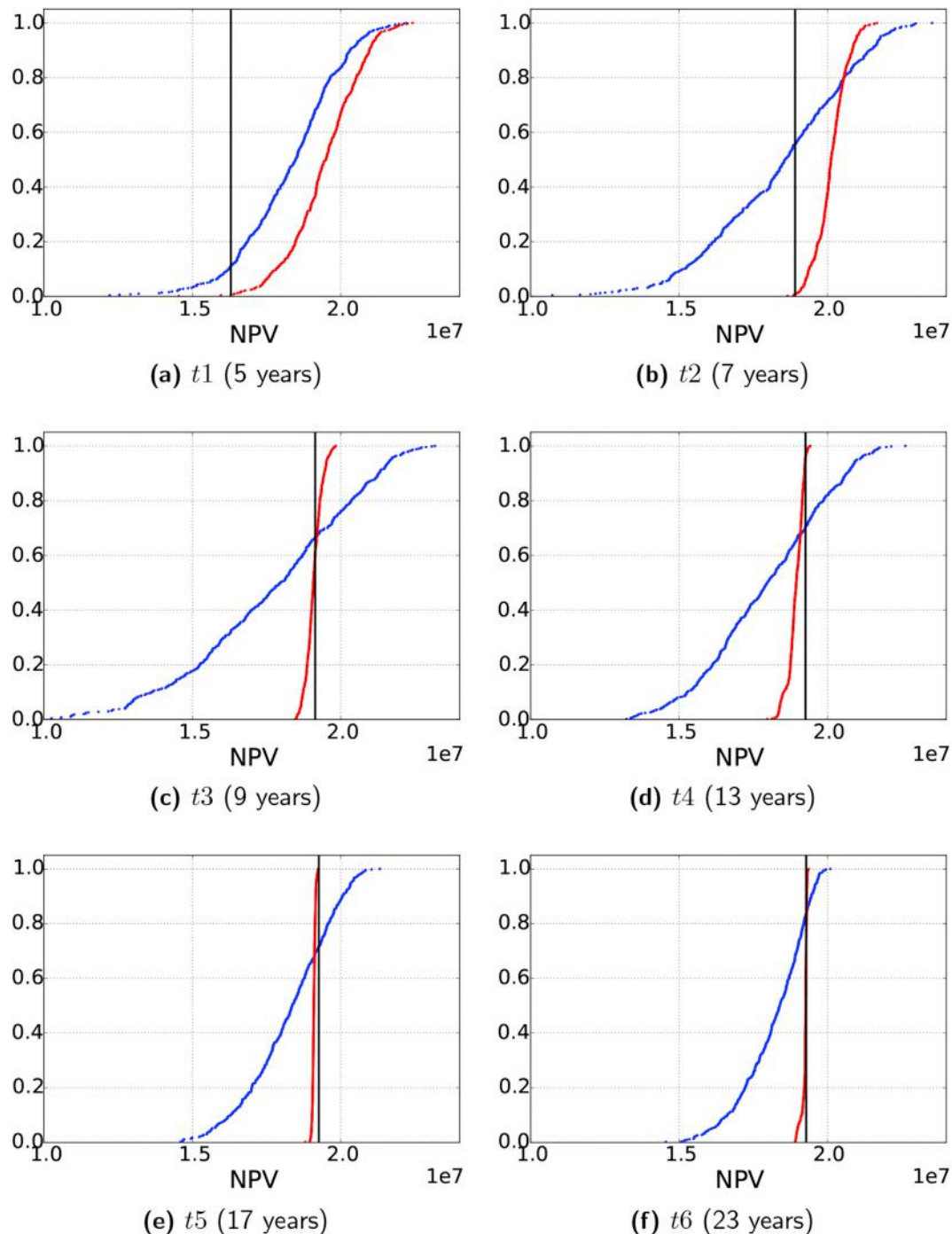


**Fig. 5.** Cumulative distributions of the predicted NPV from the prior (in blue) and the posterior (in red) ensembles for each historical period. The vertical black line represent the NPV of UNISIM-I-R. (For interpretation of the references to colour in this figure legend, the reader is referred to the web version of this article.)

**Table 3**
Selection variables and respective weights.

| Grid parameters | | | | Scalar parameters | | Production and volume variables | |
|---|---|---|---|---|---|---|---|
| $k_{I,mean}$ | 1 | $k_{I,std}$ | 1 | MULTK | 1 | OOIP | 1 |
| $k_{J,mean}$ | 1 | $k_{J,std}$ | 1 | SWCR | 1 | Np | 3 |
| $k_{Z,mean}$ | 1 | $k_{Z,std}$ | 1 | KRWMAX | 1 | Wp | 3 |
| $\phi_{mean}$ | 1 | $\phi_{std}$ | 1 | CPOR | 1 | RF | 3 |
| $ntg_{mean}$ | 1 | $ntg_{std}$ | 1 | WOC2 | 1 | VPL | 7 |

**Table 4**
Selected models and respective probabilities.

| Selected models | Probability |
|---|---|
| 142 | 19.6% |
| 220 | 23.0% |
| 225 | 22.8% |
| 338 | 16.0% |
| 475 | 18.6% |
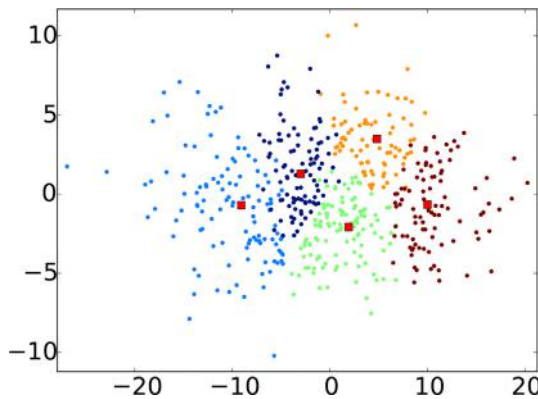


**Fig. 6.** Result of the MDS applied to the 500 realizations of UNISIM-I-D after history matching (t1). The squares in red represent the selected models. The different colors correspond to the clusters of models. (For interpretation of the references to colour in this figure legend, the reader is referred to the web version of this article.)

their corresponding final probabilities.

In order to evaluate the performance of the model selection procedure, we applied multidimensional scaling (MDS) (Borg and Groenen, 2005) using the same metric used for model selection. MDS has been used in the context of history matching and models selection for various authors; see, e.g., (Scheidt and Caers, 2009b, a; Hajizadeh et al., 2012). Fig. 6 shows the result of the MDS highlighting the five selected models. The distances between points on the MDS plot can be interpreted as a measure of dissimilarity. Points close in the plot are assumed to correspond to models with similar behaviour. This figure shows that the selected models are well distributed over the set of 500 realizations. In this figure, we also show in different colors the clusters of models corresponding to each selected model. Another way to visualize how representative are the selected models is by cross-plotting selection variables (two variables per plot). Fig. 7 presents some of these cross-plots showing that the selection procedure resulted in models distributed throughout the entire spread of the variables.

## 5. Production optimization

The production optimization problem of interest in this paper can be stated as

$$\max_{\mathbf{u}} \mathscr{F}(\mathbf{u}) \tag{8}$$

s.t. $\mathbf{u}^{low} \leq \mathbf{u} \leq \mathbf{u}^{up}$,

where $\mathscr{F}(\mathbf{u})$ is the production objective function and $\mathbf{u}$ is the vector of control variables. Here, the control variables correspond to ICV settings for all wells at a discrete set of time steps uniformly spaced throughout the entire production period. $\mathbf{u}^{low}$ and $\mathbf{u}^{up}$ are the lower and upper bound constraints, respectively. We solve this problem with the EnOpt method with the implementation developed by (Oliveira, 2014). EnOpt is based on sampling a set of "perturbed controls" around the current set of controls to define a search direction. EnOpt uses the following iterative update scheme

$$\mathbf{u}^{k+1} = \mathbf{u}^k + \beta_k \delta \mathbf{u}^k, \tag{9}$$

where $k$ is the iteration index, $\beta_k$ is the step size and $\delta \mathbf{u}^k$ is the search direction, which is calculated as

$$\delta \mathbf{u}^k = \frac{\mathbf{C_u C}_{\mathbf{u}\mathscr{F}}^k}{\left\| \mathbf{C_u C}_{\mathbf{u}\mathscr{F}}^k \right\|_\infty}. \tag{10}$$

In the above equation, $\mathbf{C_u}$ is the covariance matrix of the control variables. Here, we assume that controls are correlated over a period of five years (five control steps). The entries of $\mathbf{C_u}$ are computed using a spherical covariance function with unity variance, i.e.,

$$\mathbf{C}_{\mathbf{u}_{ij}} = \mathrm{cov}\left[\mathbf{u}_i, \mathbf{u}_j\right] = \begin{cases} 1 - \frac{3}{2}\frac{|i-j|}{T} + \frac{1}{2}\frac{|i-j|^3}{T^3} & \text{if } |i-j| < T \\ 0 & \text{if } |i-j| \geq T \end{cases}, \tag{11}$$

where $i$ and $j$ denote the $i$th and $j$th control steps and $T$ is the correlation length (given in terms of the number of control steps). In addition, the controls are assumed to be correlated only over time, i.e., there is no prior correlation between controls at different locations (different ICVs). $\mathbf{C_u}$ works as an regularization matrix applied to the search direction enforcing the optimization to generate smooth control changes; see, e.g., (Oliveira et al., 2015) for a more detailed discussion about the effect of $\mathbf{C_u}$.

In Eq. (10), $\mathbf{C}_{\mathbf{u}\mathscr{F}}^k$ represents a cross-covariance between controls and the objective function, which is computed as

$$\mathbf{C}_{\mathbf{u}\mathscr{F}}^k = \frac{1}{N_p} \sum_{j=1}^{N_p} \left(\tilde{\mathbf{u}}_j - \mathbf{u}^k\right)\left(\mathscr{F}(\tilde{\mathbf{u}}_j) - \mathscr{F}(\mathbf{u}^k)\right)^{\mathrm{T}}, \tag{12}$$

where $N_p = 10$ is the number of perturbed controls, $\tilde{\mathbf{u}}_j$, which are computed by sampling a multivariate Gaussian distribution with mean given by the current set of controls, $\mathbf{u}^k$, and covariance $\mathbf{C_u}$, i.e., $\tilde{\mathbf{u}}_j \sim \mathscr{N}(\mathbf{u}^k, \mathbf{C_u})$. Note that because $\mathscr{F}(\cdot)$ is a scalar function of $\mathbf{u}$, Eq. (12) results in a column vector with the same dimension of $\mathbf{u}$. Here, we intentionally write $\mathscr{F}(\cdot)$ as a function only of the controls, $\mathbf{u}$, to emphasize that the vector of model parameters, $\mathbf{m}$, is fixed during the EnOpt iterative process. This is different from the approaches used in (Chen et al., 2009; Fonseca et al., 2017) where both model parameters and controls are sampled in order to estimate the search direction for robust optimization.

Eq. (9) requires the computation of a step size for each iteration of EnOpt. Typically, the step size is computed by solving a line search problem. Here, because we execute simulations on a cluster of computers, we simply compute $\mathscr{F}(\mathbf{u}^k + \beta_k \delta \mathbf{u}^k)$ for ten discrete values of $\beta_k$ and choose the highest one. Similar to Zhao et al. (2013), we use three termination criteria for the optimization:

1. If the highest objective function found in the line search is not higher than the current optimal control, i.e., $\mathscr{F}(\mathbf{u}^{k+1}) \leq \mathscr{F}(\mathbf{u}^k)$, we generate a new set of perturbed controls for use in Eq. (12) and perform a new
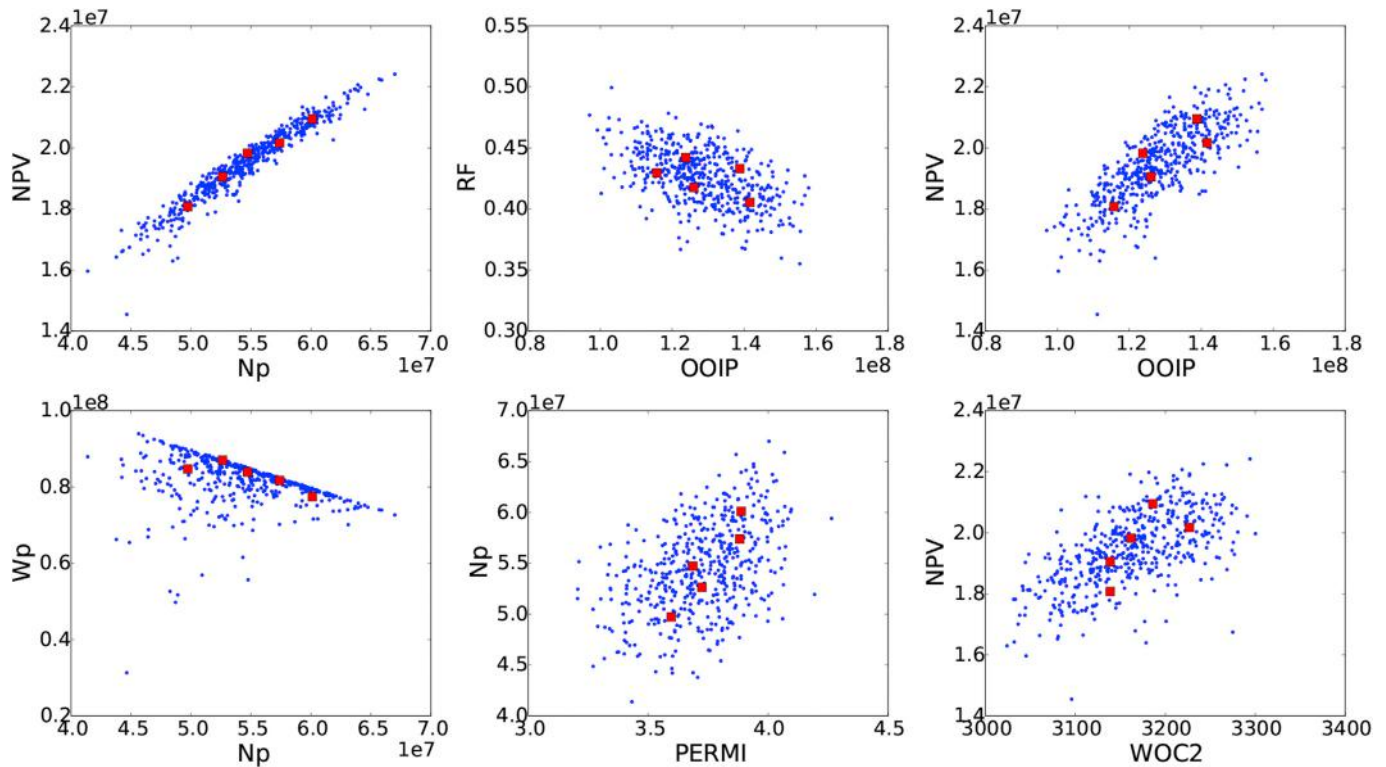
**Fig. 7.** Cross-plot of selection variables. The squares in red represent the selected models while the points in blue represent the entire ensemble. (For interpretation of the references to colour in this figure legend, the reader is referred to the web version of this article.)

line search. If after three successive line searches a new set of controls that improves the objective function is not found, then the algorithm is terminated.

2. If the relative increase in the objective function is less than $10^{-4}$,

$$\frac{|\mathscr{F}(\mathbf{u}^{k+1}) - \mathscr{F}(\mathbf{u}^{k})|}{\mathscr{F}(\mathbf{u}^{k})} \leq 10^{-4}, \qquad (13)$$

and the $\ell^2 -$ norm of the relative change in the vector of control variables is less than $10^{-3}$,

$$\frac{\|\mathbf{u}^{k+1} - \mathbf{u}^{k}\|_2}{\max\{\|\mathbf{u}^{k}\|_2 ; 1\}} \leq 10^{-3}, \qquad (14)$$

then the algorithm is terminated.

3. If the number of objective function evaluations is higher than 2,000, then the algorithm is terminated.

Our experience with EnOpt and other gradient-free optimization techniques is that the performance may be very dependent on the choice of internal parameters of the method. Our setup of EnOpt is based on our previous experience with this method in other optimization problems. Because of the stochastic formulation, the optimization results are also dependent of the random seed used to initiate the algorithm. Nevertheless, we did not perform additional experimentations to tune EnOpt specifically for the UNISIM-I case.

Before we introduce the final CLRM workflow, we first investigate the performance of EnOpt to maximize the field NPV in the UNISIM-I problem (open-loop optimizations). We conducted this investigation considering the posterior ensemble after history matching a five-years

production period (i.e., end of cycle $t1$). The control variables for optimization correspond to two ICVs per well for all 25 wells in the field. Here, the time interval of control changes is one year and the total production period where we control the ICVs is 23 years. Therefore, this problem corresponds to a total of 1150 variables. The ICVs are modeled as multipliers varying between 0 and 1 applied to the well index. During optimizations, we ensure that the multipliers are in the expected range $[0, 1]$ using the following logit transform

$$u_i = \ln\left(\frac{x_i}{1 - x_i}\right), \qquad (15)$$

where $x_i$ is the $i$th well index multiplier and $u_i$ is the corresponding transformed variable that can vary from $-\infty$ to $+\infty$. With this transformation of variables, we convert the original constrained problem of Eq. (8) to an unconstrained problem. The starting point of all optimizations is $u_i = 0$, i.e., $x_i = 0.5$, since near the bounds, $u_i \rightarrow \pm\infty$, the objective function becomes extremely insensitive to changes in $u_i$.

A typical approach for optimization considering uncertainty is to define the objective function as the expected NPV (ENPV) computed over a set of realizations. Here, we compute ENPV based on the five selected models with their respective final probabilities as described in the previous section. Hence, we define our production objective function as

$$\mathscr{F}(\mathbf{u}) \equiv \text{ENPV} = \sum_{j=1}^{5} q_j \mathscr{J}(\mathbf{m}_j, \mathbf{u}). \qquad (16)$$

For comparisons, we also conducted optimizations for each of the five selected models and one optimization for the average model, i.e., we also consider the following objective functions

**Table 5**
NPV (in millions) of different production strategies applied to the five selected models.

| Production strategy | Model | | | | |
|---|---|---|---|---|---|
| | 142 | 220 | 225 | 338 | 475 |
| base | 19.05 | 18.07 | 19.83 | 20.17 | 20.95 |
| opt142 | 21.45 | 17.95 | 20.41 | 21.05 | 19.94 |
| opt220 | 19.91 | 19.53 | 20.38 | 21.10 | 21.82 |
| opt225 | 20.16 | 18.88 | 21.26 | 21.27 | 21.62 |
| opt338 | 19.87 | 18.10 | 20.10 | 21.90 | 21.22 |
| opt475 | 19.79 | 18.57 | 20.18 | 21.02 | 22.62 |
| optmean | 20.06 | 19.11 | 20.24 | 20.83 | 21.92 |
| opt5scn | 21.31 | 19.13 | 21.01 | 21.84 | 22.27 |

$$\mathcal{F}_j(\mathbf{u}) \equiv \mathcal{J}(\mathbf{m}_j, \mathbf{u}), \quad \text{for } j = 1, \ldots, 5 \tag{17}$$

and

$$\mathcal{F}_{\text{ave}}(\mathbf{u}) \equiv \mathcal{J}(\overline{\mathbf{m}}, \mathbf{u}), \tag{18}$$

where $\overline{\mathbf{m}}$ corresponds to the model with the average parameters computed over the 500 realizations.

We evaluate the effectiveness of EnOpt to optimize the UNISIM-I problem by applying the production strategy found in each case to the five representative models. Table 5 shows the NPV of these strategies. The labels opt142, opt220, opt225, opt338, opt475 stand for the production strategies optimized for models 142, 220, 225, 338 and 475, respectively. The label optmean represents the production strategy optimized for the average model and the label opt5scn represents the production strategy optimized using the ENPV. In addition to the optimized production strategies, we also include in Table 5 the results of a base (unoptimized) production strategy. This strategy corresponds to all ICVs fully opened. All strategies include a reactive control that closes the production wells when they reach a water cut of 95%.

The results of Table 5 show that the best NPV obtained for each model corresponds to the result of the production strategy obtained by optimizing the same model. For example, the production strategy with highest NPV for model 142 is opt142. This result seems obvious but we believe this is an empirical evidence that our setup of EnOpt was effective for optimizing this problem. By contrast, we could image a situation where the optimization of a model resulted in a lower NPV than the NPV obtained by applying the production strategy obtained with another model. In this anomalous case, we would conclude that optimizations were not converging properly or were trapped in local maxima. Perhaps a more important result reported in Table 5 is the fact that the production strategy obtained by optimizing the ENPV (opt5snc) is the second highest NPV for all five models. This result is an indication the opt5snc is a robust strategy for the UNISIM-I case.

Table 6 presents the predicted average NPV computed over each line of Table 5 for each production strategy. The results in this table show that the production strategy opt5scn resulted in the highest value indicating the effectiveness of this approach. This conclusion is in line with the

**Table 6**
Predicted and actual NPV (in millions).

| Production strategy | Predicted NPV (ENPV) | Actual NPV | Disappointment |
|---|---|---|---|
| base | 19.54 | 16.30 | 3.2 |
| opt142 | 20.06 | 17.87 | 2.2 |
| opt220 | 20.47 | 17.56 | 2.9 |
| opt225 | 20.57 | 17.47 | 3.1 |
| opt338 | 20.09 | 17.45 | 2.6 |
| opt475 | 20.32 | 17.22 | 3.1 |
| optmean | 20.35 | 17.73 | 2.6 |
| opt5scn | 21.00 | 18.91 | 2.1 |

results presented by van Essen et al. (2009). Table 6 also presents the actual NPV obtained by applying each production strategy to the model UNISIM-I-R. Again, opt5snc was the best production strategy. The last column of Table 6 presents the difference between the predicted and actual NPV. We refer to this difference as "disappointment." First, we note that all cases resulted in positive values for the disappointment, i.e., the predicted NPVs are higher than the actual ones. This fact can be partially explained by the fact that the posterior realizations at $t1$ seem optimistic compared to UNISIM-I-R as shown in Fig. 5(a). Nevertheless, the production strategy opt5scn is the one with lowest disappointment. Second, it is interesting to note that a positive disappointment could be expected even if the we had an unbiased ensemble at $t1$. This phenomena is reported in the literature as "optimizer's curse" or "inevitable disappointment" (Smith and Winkler, 2006; Chen and Dyer, 2009). To the best of our knowledge, the optimizer's curse was discovered by Smith and Winkler (2006) who proved that if we select alternatives using optimization based on imperfect models, we should expect to be disappointed on average, not because of any inherent bias in the estimates themselves, but because of the selection process. The results in (Smith and Winkler, 2006) also show that this effect is minimized as we improve the quality of our model, i.e., reduce prediction errors.

Fig. 8 shows the control variables resulted from the optimizations for two selected wells. The plots in this figure are presented in terms of the ICV aperture, where zero means an ICV fully closed and one means fully opened. The results of Fig. 8 illustrate the smoothing effect introduced by the covariance $\mathbf{C_u}$. Moreover, we note that each optimization resulted in significantly different production strategies, evidencing that the optimal controls are highly dependent on the model parameters. Hence, it is crucial to account for uncertainty when computing optimized controls.

## 6. Closed-loop reservoir management

In this section, we describe our closed-loop workflow based on the methods discussed in the previous sections and present the results for the UNISIM-I case. The workflow follows the well-known closed-loop flowchart introduced by Jansen et al. (2009), which is reproduced with some adaptations in Fig. 9. The part highlighted in the figure represents the real physical system (reservoir, wells and production facilities), here, represented by UNISIM-I-R. In the present study, the input of the system are the ICV settings for the producers and water injection wells and the output are measurements of bottom-hole pressure and phase rates. All measurements are corrupted with noise. One difference between Fig. 9 and the original flowchart presented by Jansen et al. (2009) is that in Fig. 9, we did not include a noise in the system input. This is because here we are able to apply the exact same optimized control in the "real system," i.e., UNISIM-I-R. However, in reality it may not be possible to impose the exact same controls used in the models in the actual production facilities. This is why the flowchart of (Jansen et al., 2009) includes a "noise" in the system input.

The central part of Fig. 9 present the models used to predict and define controls for the system. Here, these models correspond to the 500 realizations of UNISIM-I-D. These models are updated by history matching (red-loop in Fig. 9). After history matching, there is a model selection step (in green in Fig. 9). This step is not presented in the original flowchart proposed by (Jansen et al., 2009). The selected models are used in the production optimization loop (blue-loop in the figure) aiming to maximize the life-time field NPV.

In the present study, the total production period is 30 years. This period was divided into six closed-loop cycles, denoted by $t1$ to $t6$. The first cycle is after five years of production with only the original four wells of the benchmark problem. The operation of the ICVs in all 25 wells start at $t2$. The cycles $t2$, $t3$, $t4$, $t5$ and $t6$ are after 7, 9, 13, 17 and 23
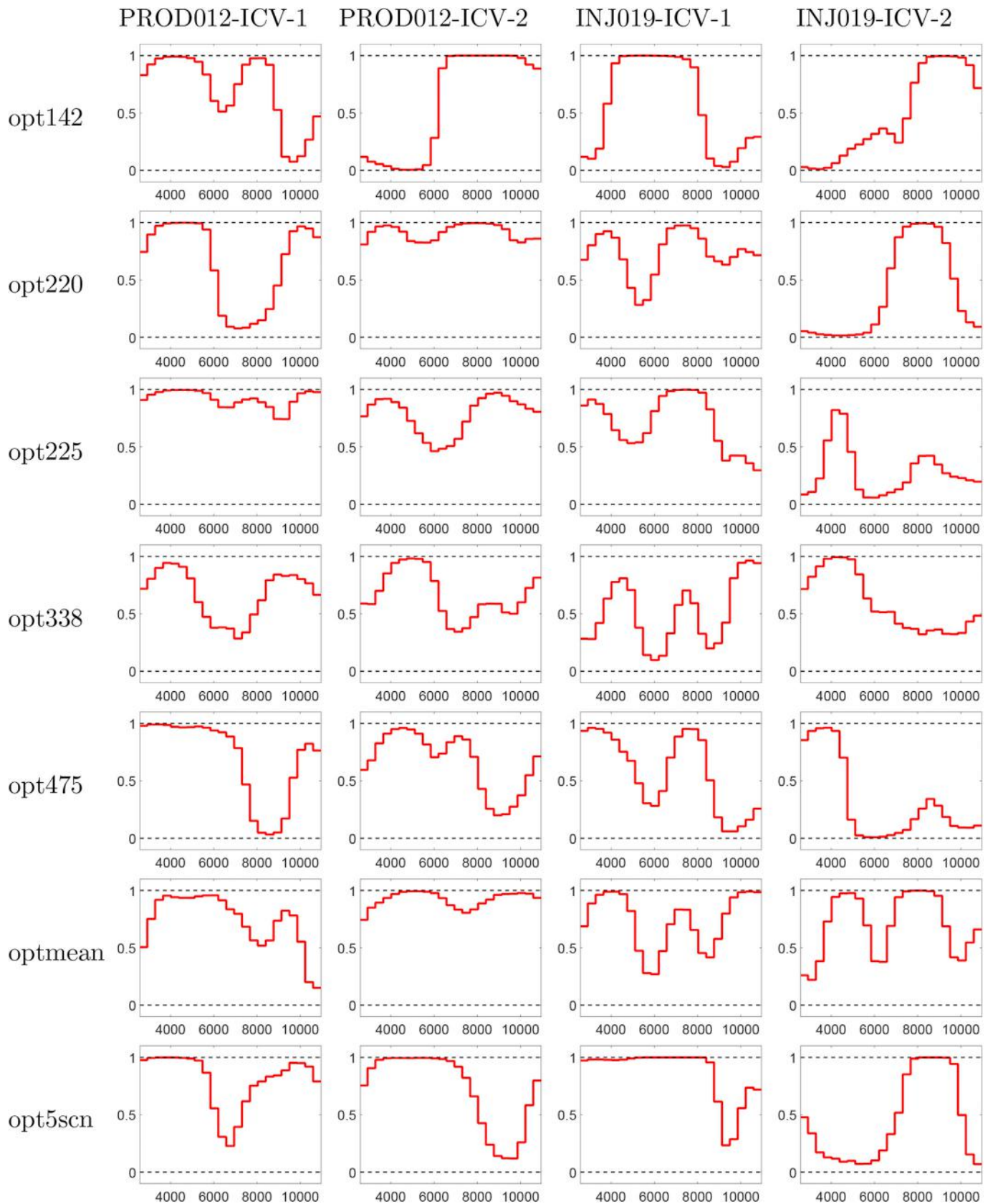
**Fig. 8.** Control variables of two wells (PROD012 and INJ019) for different production strategies. Each column corresponds to one ICV and each row to one production strategy. In each graph the horizontal axis is the time in days and the vertical axis is the ICV aperture.
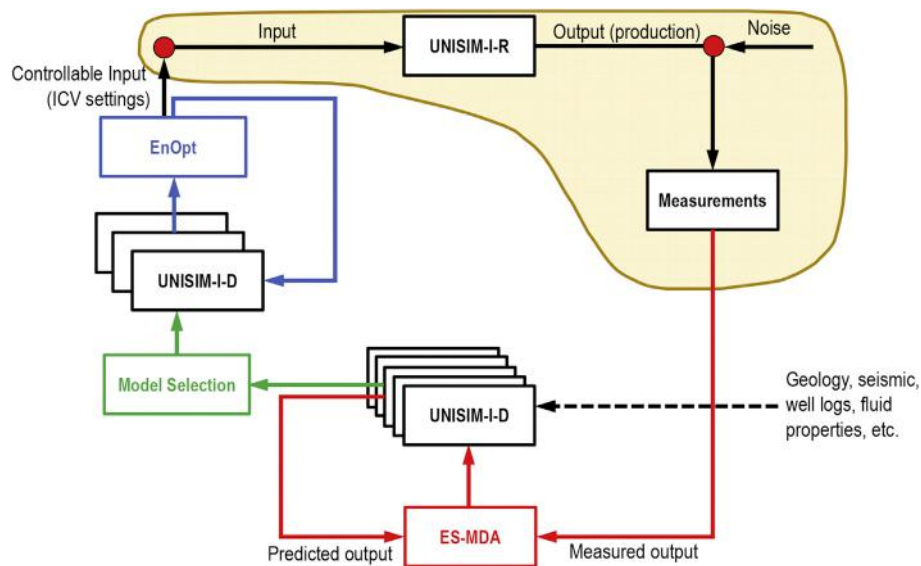
**Fig. 9.** Closed-loop reservoir management flowchart. Adapted from (Jansen et al., 2009, Fig. 1).

years of production, respectively. Even though we have only six closed-loop cycles, the ICVs settings are allowed to change once a year.

Fig. 10 presents the boxplots of predicted NPV for each cycle. These boxplots were computed applying the production strategy obtained by the optimization of the ENPV based on five representative models. We also include the actual NPV obtained by applying the optimum production strategy to the UNISIM-I-R. Fig. 10 shows that the largest improvements in NPV occurs for the early cycles. This is expected because the NPV was calculated based on the time *t*0. Therefore, the contributions of late cycles are attenuated by the effect of the discount rate. The results in Fig. 10 also show an improvement of the predictive ability of the models as the closed-loop cycles are applied. For example, initially there is a large uncertainty range in the predicted NPV and also a large difference between predicted ENPV and actual NPV (disappointment). On the other hand, for the last cycle, we have a significantly smaller uncertainty range in the predicted NPV. Perhaps more importantly, the disappointment was practically removed. It is interesting to note that a large reduction in the disappointment occurred at *t*3. Before that, at *t*2 the actual NPV was even outside of the predicted uncertainty range. This problem is essentially the same discussed after Fig. 5 where the ensemble of models resulted in biased predictions compared to UNISIM-I-R. Fig. 11 shows the evolution
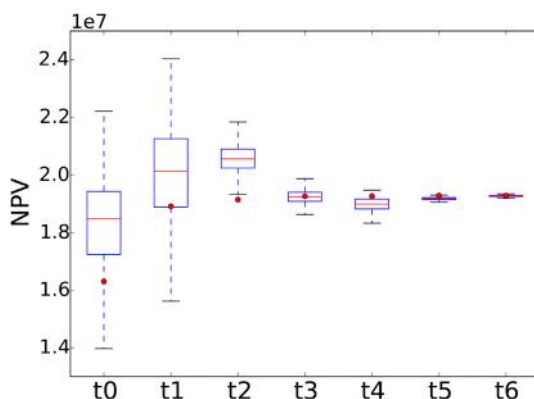
of the permeability distribution for one realization of UNISIM-I-D throughout the CLRM cycles. These results show that the changes in this model realization appear to be in the direction of reproducing the main features of the UNISIM-I-R model.

Fig. 12 shows a comparison between the open-loop optimization strategies described in previous section and the CLRM production strategy applied to UNISIM-I-R. The results in this figure show that the CLRM obtained the best NPV with approximately 18.3% gain compared to the base strategy. As a final comparison, we also computed the optimum production strategy by running an open-loop optimization with EnOpt applied directly to UNISIM-I-R. This strategy is labeled as optreal in Fig. 12. Because of the large size of this model, this optimization required almost two months of computation in a cluster. The NPV value found in this optimization can be interpreted as the maximum achievable value with our optimization setup. The difference between this value and the value obtained by the CLRM strategy was only 1%, showing the consistency of the proposed CLRM workflow. A somewhat surprising result is that the production strategy opt5scn also achieved reasonable NPV values, 1.9% less than the CLRM strategy and 2.9% less that optreal. Recall that the strategy opt5scn was obtained with the models at the cycle *t*1. These models presented a large uncertainty range and a tendency to overestimate production (large disappointment). Although we cannot generalize conclusions based on a single experiment, this result may be seen as an empirical evidence that model-based production optimization strategies can bring value to the field even in the early stages of production where the uncertainties are large. In our results, the biggest difference between CLRM and opt5scn is the reduction of the disappointment due to the improvement of the quality of the model predictions because of the history matching.

The results obtained in this paper agree with the results published by other researchers. For example, several authors (Brouwer et al., 2004; Sarma et al., 2008b; Jansen et al., 2009; Chen et al., 2010; Chen and Oliver, 2010) showed that CLRM resulted in significant increase in NPV compared to reactive control strategies. Chen and Oliver (2010) also concluded that the combination of ensemble-based data assimilation and optimization performed very well resulting in a disappointment of only 1% when simulating the optimized controls in the reference model with known geology. Other authors (Brouwer et al., 2004; Sarma et al., 2005, 2008b; Jansen et al., 2009) also concluded that CLRM resulted in a final NPV close to the one obtained in a open-loop optimization with the reference model.
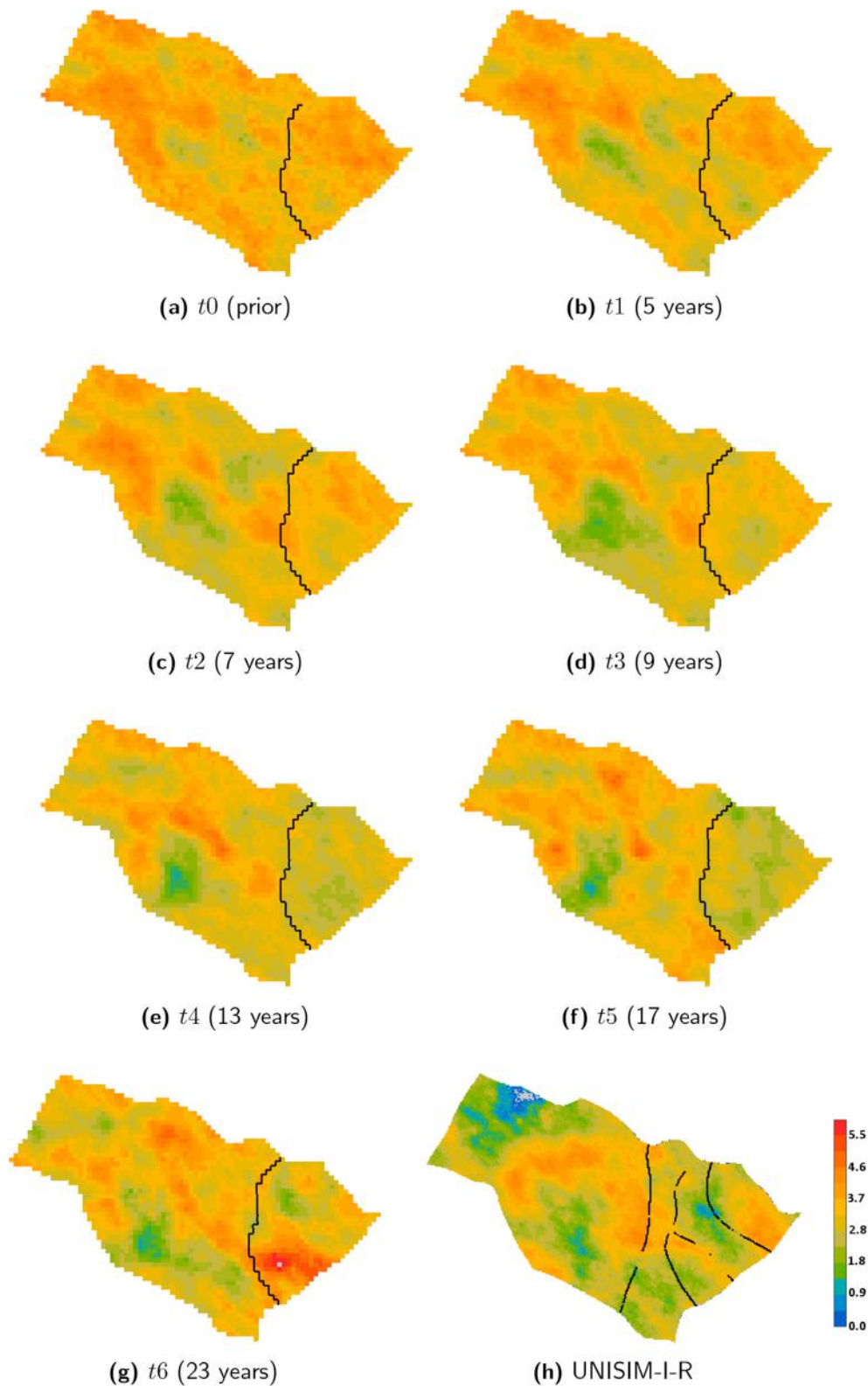


**Fig. 10.** Box-plots of predicted NPV for each closed-loop cycle computed over the 500 model realizations of UNISIM-I-D. The red circles represent the actual NPV obtained with UNISIM-I-R. (For interpretation of the references to colour in this figure legend, the reader is referred to the web version of this article.)

**Fig. 11.** Average log-permeability (in ln-mD) distribution of the first realization of UNISIM-I-D after each closed-loop cycle.

## 7. Conclusion

In this work, we proposed a closed-loop workflow combining the method ES-MDA for history matching, followed by a selection procedure to choose a subset of representative models for production optimization with EnOpt. We tested the proposed workflow in the UNISIM-I benchmark problem. We demonstrated the performance of each method separately before showing the results combined in a closed-loop. The results showed consistent improvements in the predictive ability of the models during the closed-loop cycles. The final NPV attained by the
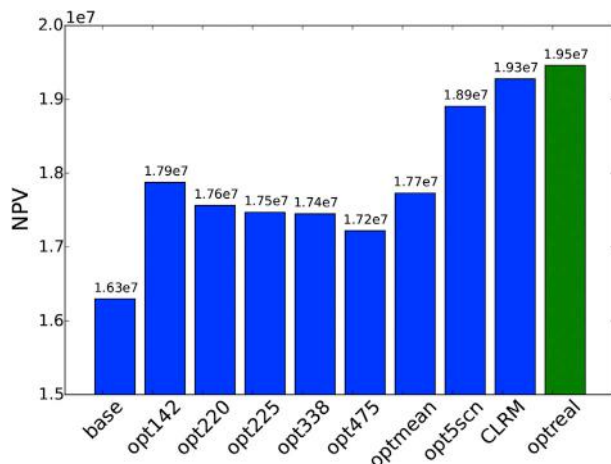
**Fig. 12.** NPV of different production strategies applied to UNISIM-I-R.

closed-loop was superior to the NPV obtained with open-loop optimizations and only 1% bellow the NPV obtained by optimization of the reference reservoir model.

## References

Aanonsen, S.I., Nævdal, G., Oliver, D.S., Reynolds, A.C., Vallès, B., 2009. Review of ensemble Kalman filter in petroleum engineering. SPE J. 14 (3), 393–412. http://dx.doi.org/10.2118/117274-PA.

Armstrong, M., Ndiaye, A., Razanatsimba, R., Galli, A., 2013. Scenario reduction applied to geostatistical simulations. Math. Geol. 45, 165–182. http://dx.doi.org/10.1007/s11004-012-9420-7.

Armstrong, M., Vincent, A., Galli, A.G., Méheut, C., 2014. Genetic algorithms and scenario reduction. J. South. Afr. Inst. Min. Metall. 114 (3), 237–244.

Avansi, G.D., Schiozer, D.J., 2015. UNISIM-I: synthetic model for reservoir development and management applications. Int. J. Model. Simul. Petrol. Ind. 9 (1), 21–30. http://www.ijmspi.org/ojs/index.php/ijmspi/article/view/152.

Ballin, P.R., Journel, A.G., Aziz, K., 1992. Prediction of uncertainty in reservoir performance forecast. J. Can. Petrol. Technol. 31 (4), 52–62. http://dx.doi.org/10.2118/92-04-05.

Borg, I., Groenen, P.J.F., 2005. Modern Multidimensional Scaling: Theory and Applications, 2 edition. Springer-Verlag, New York. http://dx.doi.org/10.1007/0-387-28981-X.

Brouwer, D.R., Nævdal, G., Jansen, J.D., Vefring, E.H., van Kruijsdijk, C.P.J.W., 2004. Improved reservoir management through optimal control and continuous model updating. In: Proceedings of the SPE Annual Technical Conference and Exhibition. http://dx.doi.org/10.2118/90149-MS. Houston, Texas, 26-29 September, number SPE 90149.

Chen, C., Li, G., Reynolds, A., 2012. Robust constrained optimization of short- and long-term net present value for closed-loop reservoir management. SPE J. 17 (3), 849–864. http://dx.doi.org/10.2118/141314-PA.

Chen, C., Li, G., Reynolds, A.C., 2010. Closed-loop reservoir management on the Brugge test case. Comput. Geosci. 14 (4), 691–703. http://dx.doi.org/10.1007/s10596-010-9181-7.

Chen, M., Dyer, J., 2009. Inevitable disappointment in projects selected on the basis of forecasts. SPE J. 14 (2), 216–221. http://dx.doi.org/10.2118/107710-PA.

Chen, Y., Oliver, D.S., 2010. Ensemble-based closed-loop optimization applied to Brugge field. SPE Reserv. Eval. Eng. 13 (1), 56–71. http://dx.doi.org/10.2118/118926-PA.

Chen, Y., Oliver, D.S., 2012. Ensemble randomized maximum likelihood method as an iterative ensemble smoother. Math. Geosci. 44 (1), 1–26. http://dx.doi.org/10.1007/s11004-011-9376-z.

Chen, Y., Oliver, D.S., Zhang, D., 2009. Efficient ensemble-based closed-loop production optimization. SPE J. 14 (4), 634–645. http://dx.doi.org/10.2118/112873-PA.

Do, S.T., Reynolds, A.C., 2013. Theoretical connections between optimization algorithms based on an approximate gradient. Comput. Geosci. 17 (6), 959–973. http://dx.doi.org/10.1007/s10596-013-9368-9.

Emerick, A.A., 2016. Analysis of the performance of ensemble-based assimilation of production and seismic data. J. Petrol. Sci. Eng. 139, 219–239. http://dx.doi.org/10.1016/j.petrol.2016.01.029.

Emerick, A.A., Reynolds, A.C., 2011a. Combining sensitivities and prior information for covariance localization in the ensemble Kalman filter for petroleum reservoir applications. Comput. Geosci. 15 (2), 251–269. http://dx.doi.org/10.1007/s10596-010-9198-y.

Emerick, A.A., Reynolds, A.C., 2011b. History matching a field case using the ensemble Kalman filter with covariance localization. SPE Reserv. Eval. Eng. 14 (4), 423–432. http://dx.doi.org/10.2118/141216-PA.

Emerick, A.A., Reynolds, A.C., 2013a. Ensemble smoother with multiple data assimilation. Comput. Geosci. 55, 3–15. http://dx.doi.org/10.1016/j.cageo.2012.03.011.

Emerick, A.A., Reynolds, A.C., 2013b. History matching of production and seismic data for a real field case using the ensemble smoother with multiple data assimilation. In: Proceedings of the SPE Reservoir Simulation Symposium. http://dx.doi.org/10.2118/163675-MS. The Woodlands, Texas, USA, 18–20 February, number SPE 163675.

Emerick, A.A., Reynolds, A.C., 2013c. Investigation on the sampling performance of ensemble-based methods with a simple reservoir model. Comput. Geosci. 17 (2), 325–350. http://dx.doi.org/10.1007/s10596-012-9333-z.

Evensen, G., 1994. Sequential data assimilation with a nonlinear quasi-geostrophic model using Monte Carlo methods to forecast error statistics. J. Geophys. Res. 99 (C5), 10143–10162. http://dx.doi.org/10.1029/94JC00572.

Fonseca, R.M., Chen, B., Jansen, J.D., Reynolds, A.C., 2017. A stochastic simplex approximate gradient (StoSAG) for optimization under uncertainty. Int. J. Numer. Methods Eng. 109 (13), 1756–1776. http://dx.doi.org/10.1002/nme.5342.

Gaspar, A.T., Avansi, G.D., Santos, A.A.S., von Hohendorff Filho, J.C., Schiozer, D.J., 2015. UNISIM-I-D: benchmark studies for oil field development and production strategy selection. Int. J. Model. Simul. Petrol. Ind. 9 (1), 47–55. http://www.ijmspi.org/ojs/index.php/ijmspi/article/view/173.

Gaspari, G., Cohn, S.E., 1999. Construction of correlation functions in two and three dimensions. Q. J. R. Meteorol. Soc. 125 (554), 723–757. http://dx.doi.org/10.1002/qj.49712555417.

Hajizadeh, Y., Amorim, E., Sousa, M.C., 2012. Building trust in history matching: the role of multidimensional projection. In: Proceedings of the SPE Europec/EAGE Annual Conference. http://dx.doi.org/10.2118/152754-MS, 4-7 June, Copenhagen, Denmark, number SPE 152754.

Heitsch, H., Römisch, W., 2003. Scenario reduction algorithms in stochastic programming. Comput. Optim. Appl. 24 (2), 187–206. http://dx.doi.org/10.1023/A:1021805924152.

Jansen, J.D., 2011. Adjoint-based optimization of multi-phase flow through porous media – a review. Comput. Fluids 46 (1), 40–51. http://dx.doi.org/10.1016/j.compfluid.2010.09.039.

Jansen, J.D., Douma, S.D., Brouwer, R., den Hof, P.M.J.V., Heemink, A.W., 2009. Closed-loop reservoir management. In: Proceedings of the SPE Reservoir Simulation Symposium. http://dx.doi.org/10.2118/119098-MS. The Woodlands, Texas, 2–4 February, number SPE 119098.

Kalman, R.E., 1960. A new approach to linear filtering and prediction problems. Transactions of the ASME. J. Basic Eng. 82, 35–45.

Lorentzen, R.J., Berg, A.M., Nævdal, G., Vefring, E.H., 2006. A new approach for dynamic optimization of waterflooding problems. In: Proceedings of the SPE Intelligent Energy Conference and Exhibition. http://dx.doi.org/10.2118/99690-MS number SPE 99690.

Maucec, M., Ravanelli, F.M.D.M., Lyngra, S., Zhang, S.J., Alramadhan, A.A., Abdelhamid, O.A., Al-Garni, S.A., 2016. Ensemble-based assisted history matching with rigorous uncertainty quantification applied to a naturally fractured carbonate reservoir. In: Proceedings of the SPE Annual Technical Conference and Exhibition. http://dx.doi.org/10.2118/181325-MS. Dubai, UAE, 26–28 September, number SPE 181325.

Meira, L.A.A., Coelho, G.P., Santos, A.A.S., Schiozer, D.J., 2016. Selection of representative models for decision analysis under uncertainty. Comput. Geosci. 88, 67–82. http://dx.doi.org/10.1016/j.cageo.2015.11.012.

Nocedal, J., Wright, S.J., 2006. Numerical Optimization. Springer, New York.

Oliveira, D.F.B., 2014. A New Hierarchical Multiscale Optimization Method: Gradient and Non-gradient Approaches for Waterflooding Optimization. PhD thesis. The University of Tulsa.

Oliveira, D.F.B., Reynolds, A.C., Jansen, J.D., 2015. An improved multiscale method for life-cycle production optimization. Comput. Geosci. 19 (6), 1139–1157. http://dx.doi.org/10.1007/s10596-015-9530-7.

Oliveira, W.L., Claudia Sagastizábal, D.D.J.P., Maceira, M.E.P., Damázio, J.M., 2010. Optimal scenario tree reduction for stochastic streamflows in power generation planning problems. Optim. Methods Softw. 25 (6), 917–936. http://dx.doi.org/10.1080/10556780903420135.

Oliver, D.S., Chen, Y., 2011. Recent progress on reservoir history matching: a review. Comput. Geosci. 15 (1), 185–221. http://dx.doi.org/10.1007/s10596-010-9194-2.

Reynolds, A.C., Zafari, M., Li, G., 2006. Iterative forms of the ensemble Kalman filter. In: Proceedings of 10th European Conference on the Mathematics of Oil Recovery. http://dx.doi.org/10.3997/2214-4609.201402496. Amsterdam, 4–7 September.

Rommelse, J., 2009. Data Assimilation in Reservoir Management. Ph.D. thesis. Technical University of Delft, Delft, The Netherlands.

Sarma, P., Chen, W.H., Durlofsky, L.J., Aziz, K., 2008a. Production optimization with adjoint models under nonlinear control-state path inequality constraints. SPE Reserv. Eval. Eng. 11 (2), 326–339. http://dx.doi.org/10.2118/99959-PA.

Sarma, P., Durlofsky, L.J., Aziz, K., 2005. Efficient closed-loop production optimization under unceratinty. In: Proceedings of the SPE/EAGE Annual Conference. http://dx.doi.org/10.2118/94241-MS number SPE 94241.

Sarma, P., Durlofsky, L.J., Aziz, K., 2008b. Computational techniques for closed-loop reservoir modeling with application to a realistic reservoir. Petrol. Sci. Technol. 26 (10–11), 1120–1140. http://dx.doi.org/10.1080/10916460701829580.

Scheidt, C., Caers, J., 2009a. Representing spatial uncertainty using distances and kernels. Math. Geol. 41 (4), 397–419. http://dx.doi.org/10.1007/s11004-008-9186-0.

Scheidt, C., Caers, J., 2009b. Uncertainty quantification in reservoir performance using distances and kernel methods–application to a West Africa deepwater turbidite reservoir. SPE J. 14 (4), 680–692. http://dx.doi.org/10.2118/118740-PA.

Schiozer, D., Ligero, E., Suslick, S., Costa, A., Santos, J., 2004. Use of representative models in the integration of risk analysis and production strategy definition. J. Petrol. Sci. Eng. 44 (1–2), 131–141. http://dx.doi.org/10.1016/j.petrol.2004.02.010.

Shirangi, M.G., Durlofsky, L.J., 2016. A general method to select representative models for decision making and optimization under uncertainty. Comput. Geosci. 96, 109–123. http://dx.doi.org/10.1016/j.cageo.2016.08.002.

Skjervheim, J.-A., Evensen, G., Hove, J., Vabø, J.G., 2011. An ensemble smoother for assisted history matching. In: Proceedings of the SPE Reservoir Simulation Symposium. http://dx.doi.org/10.2118/141929-MS. The Woodlands, Texas, USA, 21–23 February, number SPE 141929.

Smith, J.E., Winkler, R.L., 2006. The optimizer's curse: skepticism and postdecision surprise in decision analysis. Manag. Sci. 52 (3), 311–322. http://dx.doi.org/10.1287/mnsc.1050.0451.

Spall, J.C., 1992. Multivariate stochastic approximation using a simultaneous perturbation gradient approximation. IEEE Trans. Autom. Control. 37 (3), 332–341. http://dx.doi.org/10.1109/9.119632.

Spall, J.C., 1998. Implementation of the simultaneous perturbation algorithm for stochastic optimization. IEEE Trans. Aerosp. Electron. Syst. 34 (3), 817–823. http://dx.doi.org/10.1109/7.705889.

van Essen, G., Zandvliet, M., den Hof, P.V., Bosgra, O., Jansen, J.D., 2009. Robust waterflooding optimization of multiple geological scenarios. SPE J. 14 (1), 202–210. http://dx.doi.org/10.2118/102913-PA. http://dx.doi.org/10.2118/102913-PA.

van Leeuwen, P.J., Evensen, G., 1996. Data assimilation and inverse methods in terms of a probabilistic formulation. Mon. Weather Rev. 124, 2898–2913. http://dx.doi.org/10.1175/1520-0493(1996)124<2898:DAAIMI>2.0.CO;2.

Wang, C., Li, G., Reynolds, A.C., 2009. Production optimization in closed-loop reservoir management. SPE J. 14 (3), 506–523. http://dx.doi.org/10.2118/109805-PA.

Zhao, H., Chen, C., Do, S.T., Oliveira, D.F.B., Li, G., Reynolds, A.C., 2013. Maximization of a dynamic quadratic interpolation model for production optimization. SPE J. 18 (6), 1012–1025. http://dx.doi.org/10.2118/141317-PA.